Single-molecule imaging of eukaryotic replisomes reveals compositional plasticity

Jacob S. Lewis[1,2]*, Lisanne M. Spenkelink[1,2]*, Grant D. Schauer[3], Olga Yurieva[3,4], Varsha Natarajan[1,2], Gurleen Kaur[1,2] , Claire Maher[1,2], Callum Kay[1,2], Michael E. O'Donnell[3,4], Antoine M. van Oijen[1,2].

[1]Molecular Horizons and School of Chemistry and Molecular Bioscience, University of Wollongong, Wollongong, New South Wales, 2522, Australia. [2]Illawarra Health & Medical Research Institute, Wollongong, New South Wales, 2522, Australia. [3]Laboratory of DNA Replication, Rockefeller University, New York, NY 10065.[4]Howard Hughes Medical Institute.

*These authors contributed equally to this work

Summary

Duplication of the chromosomal DNA prior to cell division is performed by the replisome, a multi-protein complex that coordinates a large number of enzymatic activities. The eukaryotic replisome couples unwinding by the replicative DNA helicase (CMG) with the synthesis activity of DNA polymerases α, δ, and ε to simultaneously duplicate the leading and lagging strands. The ensemble-averaging nature of biochemical experiments obscures details on kinetics and stoichiometry of multi-protein complexes and makes it challenging to determine the exact composition of the replisome during replication and whether protein components might dynamically be exchanged. Here we describe fluorescence imaging of the eukaryotic replisome reconstituted from purified proteins and visualised at the single-molecule level while replicating DNA. We find that the two processive replicative DNA polymerases Pol ε and Pol δ exchange stochastically and in a concentration-dependent

manner, suggesting that the interactions within the replisome are optimised to balance stability with plasticity. We further show that Pol δ synthesizes multiple Okazaki fragments while remaining attached to the replisome, facilitated by interaction with Pol α.

Introduction

The eukaryotic replisome contains three different multi-subunit B-family DNA polymerases — Pol ε, Pol δ, and Pol α, with Pol ε synthesising leading-strand DNA, Pol δ to support synthesis of the lagging strand, and Pol α responsible for primer synthesis [1]. A strong interaction between Pol ε and the CMG helicase [2,3] provides high processivity on the leading strand. Lagging-strand synthesis requires repeated cycles of production of ~25 nt RNA–DNA primers by Pol α and Pol δ-mediated extension of these primers to generate ~150 bp Okazaki fragments [1]. CMG is required for Pol α priming function, suggesting that Pol α has a specific interaction with CMG [4]. Furthermore, Ctf4 and Mcm10 are known to bind both Pol α and CMG [5,6]. Together, these interactions tether Pol α to CMG for replisome function during elongation. The location of the lagging-strand polymerase Pol δ within the replisome has not yet been established. There is, however, consensus that Pol δ is not physically tethered to CMG and is replaced for the synthesis of each successive Okazaki fragment.

Our understanding of the enzymatic activities and overall architecture of the eukaryotic replisome is rapidly evolving. However, the dynamic behaviour of individual proteins and complexes within the replisome remains largely unknown. Single-molecule experiments on viral and bacterial replisomes have shown a dynamic exchange of the DNA polymerases during the replication reaction, with individual polymerases entering and leaving the replisome in a concentration-dependent manner. The high stability of the replisome in the absence of polymerases in solution and the high frequency of exchange in the presence thereof suggests a compositional plasticity that allows the replisome to rapidly respond to changes in cellular conditions [7-11]. Visualising these dynamics in eukaryotic replication is key

to understanding the complex network of interactions in the replisome. Here, we report the dynamic behaviour of Pol ε and Pol δ during DNA replication by reconstituting replisomes assembled using purified proteins from budding yeast. By visualising individual Pol ε and Pol δ molecules we see clear concentration dependent exchange of both Pol ε and Pol δ during DNA synthesis. Surprisingly, Pol δ is retained at the fork on timescales consistent with multiple successive Okazaki-fragment synthesis cycles. Further, we show here that the retention of Pol δ is facilitated through interaction between the Pol32 subunit of Pol δ and the Pol 1 subunit of Pol α, shown later [12,13].

Single-molecule DNA replication

To investigate the replication kinetics of individual budding yeast replisomes, we developed a real-time single-molecule fluorescence assay allowing us to monitor both DNA synthesis and protein dynamics simultaneously. We assemble linear, double-stranded DNA (dsDNA) molecules (18.3 kb length) in a microfluidic flow cell placed onto a fluorescence microscope. The DNA is attached to the surface at both ends with the distance between attachment points such that the DNA is pulled taught. A pre-made fork at one end of the DNA with short single-stranded DNA (ssDNA) tails and a synthetic oligonucleotide primer on the leading ssDNA tail enables direct loading of the replisomal proteins onto the DNA (Fig. 1a, left, Extended Data Fig. 1). DNA synthesis was initiated by loading CMG and the Mcm10 initiation factor (CMGM) onto the template followed by the introduction of Ctf4, Mcm10, Mrc1–Tof1–Csm3 (MTC), PCNA, RFC, RPA, DNA polymerases α, δ, ε, Mg^{2+}, the four dNTPs and four rNTPs (Fig. 1a, right) [14] (see Methods for details). Real-time synthesis trajectories were obtained from near-TIRF fluorescence imaging of Sytox-orange (S.O.) stained dsDNA in the absence of buffer flow. As DNA synthesis proceeds the leading strand appears as a diffraction-limited spot that moves unidirectionally along the template DNA. Initially weak in intensity, the spot increases in intensity as more dsDNA is generated at the

leading strand and accumulates into a collapsed globular coil with dimensions smaller than the diffraction-limited spot (Fig. 1b, Supplementary Video 1). The intensity per base pair of this coiled leading-strand product is similar to the intensity per base pair as measured over the stretched template (Extended Data Fig. 2). To establish that the observed events correspond to simultaneous leading- and lagging-strand synthesis, we divided the DNA template into three regions — the leading-strand spot ('Lead'), the length of DNA behind it ('Lag') and the length ahead of it ('Parental') (Fig. 1b, right). For every time point, the DNA length is calculated from the integrated fluorescence intensity in each region [15]. The DNA content of the parental region decreased while DNA content of the leading- and lagging-strand regions increased simultaneously (Fig. 1b right, Extended Data Fig. 3). Importantly, in the absence of either Mg^{2+}, nucleotides, CMG, or DNA polymerases replication events were not observed (Extended Data Fig. 4).

To quantify the instantaneous rates of replication, we tracked the position of the leading-strand spot [16]. The measured population-averaged rate of 19 ± 6 bp/s (mean ± S.E.M.; n = 96 molecules) (Extended Data Fig. 5) is consistent with previously reported ensemble *in vitro* and *in vivo* measurements [17] [18-21]. Rates of DNA synthesis varied within individual replisomes (Fig. 1c, Extended Data Fig. 6), with the single-molecule rate distribution having two distinct peaks at 8 ± 2 bp/s and 33 ± 2 bp/s (mean ± S.E.M.; n = 96 molecules, 315 segments). This bimodal rate distribution was reported in our previous single-molecule studies of leading-strand synthesis and attributed to dynamic interaction of the MTC complex with the replisome [22]. Observation of the same rate distribution here implies MTC acts in a similar fashion during combined leading- and lagging-strand DNA synthesis.

Direct visualisation of polymerases

Enzymatic activities of both Pol ε and Pol δ are well established, but their dynamic behaviour during DNA synthesis remains unknown. To directly visualise their dynamics, as a

component of the larger replisome complex, we repeated our single-molecule assay in the presence of fluorescently labelled Pol ε and Pol δ (Fig. 2a, Extended Data Fig. 7). Labelling did not affect the average rates of DNA synthesis (Extended Data Fig. 5). The kymographs in Fig. 2b show bright fluorescent spots for both the AF488–Pol ε and Cy5–Pol δ during DNA synthesis. Both DNA polymerases co-localise with the leading-strand spot, consistent with them being incorporated into reconstituted replisomes. To calculate the stoichiometry of Pol ε and Pol δ during DNA synthesis, we divided the intensity at the fork by the intensity of a single polymerase. On average, we observe one Pol ε and one Pol δ at actively synthesising replication forks (Fig. 2c,d). This observation is consistent with a model in which both Pol ε and Pol δ are present during simultaneous synthesis of both daughter strands (Fig. 2b). In 86 ± 5% (mean ± S.E.M.; n = 70) of events DNA synthesis begins only after binding of Pol δ (Fig 2b, top). This observation is consistent with a model in which Pol δ is required for efficient leading- and lagging-strand synthesis [20,23].

Visualisation of DNA Polymerase ε dynamics

To quantify the dynamics of Pol ε, we carried out single-molecule FRAP (Fluorescence Recovery After Photobleaching) experiments [9,10,24]. Using Pol ε labeled with a red LD650 dye, we first photobleached all labelled polymerases at the replication fork using a pulse of high laser intensity (Fig. 3a, left). After bleaching, we monitored the recovery of the fluorescence as unbleached polymerases from solution exchange into the replisome (Fig. 3a, right). Fig. 3b shows a kymograph of the fluorescence recovery of Pol ε in the presence of 20 nM of Pol ε in solution. After averaging multiple real-time intensity trajectories, we obtained a characteristic exchange rate of $(12.5 \pm 0.1)\times10^{-4}$ s^{-1} (mean ± S.E.M.; n = 37, Extended Data Fig. 8. Using the synthesis rate of the replisome as discussed above, we can convert this rate constant to a characteristic length of ~15 kb. By decreasing the LD650–Pol ε concentration from 20 to 2 nM, we observed a decrease in the mean exchange rate (Fig. 3d). At the lowest

concentration of Pol ε we did not observe full fluorescence recovery on the time scale of 30 min, with only a few molecules recovering (Extended Data Fig. 8). These results show that the Pol ε exchange rate is dependent on the concentration of competing protein present in solution. Concentration-dependent exchange has previously been observed in simpler model systems such as the *E. coli* and T7 bacteriophage replisomes [7-9].

Next, we wanted to confirm that we are able to detect changes in the exchange dynamics of Pol ε by changing the biochemical processes underlying polymerase accessibility to the replisome. It has been shown that the presence of RFC clamp loader limits the access of Pol ε to the lagging strand in a quality-control mechanism that enforces the assembly of the correct polymerase for each strand [25]. We hypothesised that reducing the amount of RFC allows the leading-strand Pol ε to gain additional access to the lagging strand and thus change the observed overall exchange rate for Pol ε. We, therefore, repeated the FRAP measurements with 2 nM RFC – a concentration that is ten-fold lower than in our previous measurements (Extended Data Fig. 8). Under these conditions, there are two changes to the behaviour of Pol ε. As expected, the exchange of Pol ε is >3-fold faster compared to our previous measurements at high RFC concentrations (Fig. 3c,d). Second, at this low RFC concentration the number of Pol ε at the fork increases with increasing concentrations of Pol ε in solution (Fig. 3e). In contrast, at the higher RFC concentration there is only one Pol ε at the fork. This result is consistent with the observation that at the higher intracellular ratios of RFC to primed DNA, Pol ε is prevented from function on primed sites except when connected to CMG for leading-strand synthesis [25].

Visualisation of DNA Polymerase δ dynamics

We repeated the FRAP experiments with labelled Pol δ (Fig. 4a, Extended Data Fig. 9). Similar as observed with Pol ε, we see that the exchange rate of Pol δ is dependent on the

concentration of Pol δ in solution (Fig. 4f). Even at the highest concentration of Pol δ that still allows for visualisation of single molecules, the Pol δ exchange rate is sufficiently low to still correspond to the synthesis of many Okazaki fragments. To understand the extent to which Pol δ is recycled within the replisome to support the synthesis of multiple Okzaki fragments, we quantified the average length of Okazaki fragments under our experimental conditions. We used fluorescently labelled single-stranded DNA-binding protein RPA to assess the length of ssDNA as a measure of the Okazaki fragment size (Fig. 4c). As expected, RPA was always localised at the replication fork. Consistent with biochemical studies [14] we observe that the number of RPA molecules is dependent on the concentration of Pol α (Fig. 4c). Given that the footprint of RPA is 30 ± 2 nt (Fig. 4b) and we see 3.7 ± 0.5 (mean ± S.E.M.; n = 64) RPA molecules at the fork, we determine the Okazaki fragment length in our single-molecule experiments as 111 ± 16 bp (mean ± S.E.M.), consistent with *in vivo* studies [1]. Considering that the average rate of replication is 19 ± 6 bp/s, a new Okazaki fragment is synthesised every 6 ± 2 s. One would, therefore, expect a new Pol δ to exchange into the replisome on that same timescale. Even though Pol δ is not known to interact with CMG, our observation of slow exchange rates suggests that Pol δ is retained within the replisome to support the synthesis of multiple Okazaki fragments, and thus must have stabilising contacts with replisomal components.

We set out to identify the mechanism through which Pol δ is retained in replisomes. The Pol 32 subunit of Pol δ is documented to interact with the Pol1 subunit of Pol α [12,13]. Pol α also binds to CMG through an interaction with Ctf4 and Mcm10 [6,26]. Thus, we predicted that elimination of contact between Pol32 of Pol δ and Pol α would facilitate Pol δ dissociation from the replisome, and thus increase the exchange rate with Pol δ in solution. To test this notion, we fluorescently labelled Pol δ^{32-} (Pol δ lacking the Pol 32 subunit) and repeated the FRAP measurements (Fig. 4d, Extended Data Fig. 9). If Pol δ is indeed recycled through the

Pol32–Pol1 interaction, we predict the exchange of Pol δ^{32-} to be much faster than that of Pol δ holoenzyme (Fig. 4e). Indeed, the exchange rate of Pol δ^{32-} is $(27.0 \pm 0.5)\times10^{-4}$ s^{-1} (corresponding to a length of ~7kb) at 20 nM Pol δ^{32-} in solution (Fig. 4f). This exchange is ~2.5-fold faster than the exchange of Pol δ under the same conditions (Fig. 4f). These data indicate that without interaction with Pol α, retention of Pol δ in the replisome is significantly less efficient.

Discussion

We have reconstituted and visualised DNA synthesis by budding yeast replisomes at the single-molecule level. Our real-time single-molecule fluorescence assay allow us to directly visualise replication kinetics and protein dynamics of individual replisomes – observables that are not accessible *via* classical biochemical approaches. The average observed replication rates are similar to those previously reported in ensemble biochemical reactions [14,20,23,27] and are within the range of replication fork rates inside the cell [19,21,28]. The bimodal rate distribution observed here is consistent with our previous single-molecule leading-strand assays that identified the MTC complex as increasing the instantaneous rate of the replisome in bimodal fashion [22]. Our experiments here suggest that the same dynamic interaction is at play during leading- and lagging-strand DNA synthesis.

Based on our results, we propose the eukaryotic replisome is not fixed in composition during replication, but instead is a highly dynamic entity continually exchanging major components. This proposal is founded upon two observations (Fig. 5). (1) The leading- and lagging-strand polymerases Pol ε and Pol δ exchange during DNA synthesis in a concentration-dependent manner without affecting replication rate (Extended Data Fig. 5). (2) Pol δ can be retained at the replication fork for multiple Okazaki fragments, mediated at least in part through an interaction with Pol α.

In contrast to long-standing views that replisome architecture is static, single-molecule fluorescence experiments have documented dynamic exchange of polymerases on rapid and physiological ly relevant time scales (msec–sec) timescales [7-9]. Our work provides the first direct evidence that Pols ε and δ are similarly exchanged from solution in a concentration-dependent manner during replisome-mediated DNA synthesis. Concentration-dependent exchange can be rationalised through an interaction network consisting of multiple weak interactions. Under dilute conditions, transient disruption of any one of these interactions would be followed by its rapid re-formation and prevent dissociation. If, however, there are exogenous competitors in close proximity to the complex, one of these can bind at a transiently vacated binding site and consequently be at a sufficiently high local concentration to compete away the original protein. This concentration-dependent mechanism likely plays an important role in genomic integrity. Through such a mechanism the replisome has access to a plurality of molecular pathways to achieve and ensure continuous replisome progression under a variety of cellular stresses, for example, granting access to specialised repair polymerases or phosphorylated copies of Pol ε and Pol δ. While the current study utilises a minimal set of replisomal proteins the environment within the cell is more complex containing many additional binding partners. While these exchange processes are expected to play an important role *in vivo*, the rates of exchange may be different to the rates reported here.

It is generally assumed that Pol δ is not associated with CMG and that a new Pol δ is recruited for the synthesis of each successive Okazaki fragment. In contrast, our results show that Pol δ is retained at the fork for synthesis of multiple Okazaki fragments. This observation implies that there are one or more interactions between Pol δ and a stable part of the replisome. We show that one of these interactions is with Pol α through the Pol 32 domain of Pol δ — without this domain, Pol δ recycling is ~2.5-fold faster (Fig. 4, Fig. 5a). Pol α has a

specific interaction with CMG [14] and can be tethered to CMG *via* interactions with Ctf4 and Mcm10 [5,6]. We, therefore, propose that Pol δ is tethered to CMG mediated by the interaction with Pol α (Fig. 5b). However, Pol α is also thought to be dynamic during replisome progression and thus we expect other interactions within the replisome may contribute to the stability of Pol δ. Retention of Pol δ over the time scales presented here, along with the RPA stoichiometry during fork progression, implies that short loops are generated during replication (Fig. 5b) [29-33].

Our data suggest that the eukaryotic replisome is a system held together through a network of many pair-wise interactions. These multiple interactions give the replisome both stability and plasticity, enabling it to exploit many different molecular pathways and deal with a variety of cellular conditions. While we have used our single-molecule assay here to study polymerase dynamics, the assay is well equipped to reconstitute collisions between individual eukaryotic replisomes and other large multi-protein complexes that act on DNA, such as stalled transcription complexes. Additionally, this assay provides a novel experimental approach to study the molecular mechanisms and pathways that eukaryotic replisomes utilise to overcome template DNA damage.

Methods

Protein expression and purification

DNA replication proteins were produced as described previously: CMG, Pol ε, RFC, PCNA, and RPA [2]; Mcm10 and MTC [22,34] and Pol α, Pol δ, Ctf4 [4].

Purification of Pol δ^{32-}

Pol δ was purified as previously described [4], the final step of which involves an elution from a sulphopropyl cation exchange column (GE Healthcare) with a 100-500 mM NaCl gradient in a buffer containing 350 mM potassium glutamate and 25 mM HEPES pH 7.5. Whereas, full Pol δ elutes around 350 mM NaCl, Pol δ^{32-} elutes around 250 mM NaCl, allowing complete separation (Extended Data Fig. 10). Thus, peak fractions at 250 mM NaCl were aliquotted, flash frozen, and stored at –80°C.

Oligonucleotides and DNA

Oligonucleotides were purchased from Integrated DNA technologies (USA). Plasmid pSuperCos1 DNA was purified by Aldevron (USA).

Production of SFP synthease reagents for protein labelling

SFP synthase was purified by a nickel-NTA chromatography as previously described [35]. and Alexa Fluor 488 (AF488) was functionalized by Co-enzyme A (CoA) and purified by HPLC as previously described [35] and a LD655–CoA (a CoA-derivitized photostable version of Cy5) was purchased by Lumidyne Technologies (USA).

Preparation of LD655–Pol ε and AF488–Pol ε

To obtain Pol ε labeled with a single LD655 (Lumidyne Technologies) or Alexa Fluor 488 (Invitrogen) dye, we inserted the "S6" peptide (GDSLSWLLELLN) [36] between the N-terminus of Pol 2 and its 3× FLAG tag. The resultant Pol ε–S6 plasmid was overexpressed and purified in *S. cerevisiae* as previously described [4]. For labelling Pol ε–S6, SFP enzyme,

and either LD655–CoA or AF488–CoA were then incubated at a 1:2:5 molar ratio for 1 hour at room temperature in the presence of 10 mM $MgCl_2$. Excess dye and SFP enzyme were removed by purification on a Superose 6 column (GE Healthcare) with a buffer containing 25 mM Tris-HCl pH 7.5, 150 mM NaCl, 1 mM dithiothreitol, 5% (*v/v*) glycerol. Fractions were frozen in liquid N_2 and stored in aliquots at –80°C. The degree of labelling was determined to be ~100% for both LD655–Pol ε and A488–Pol ε by UV/vus spectrophotometry.

Preparation of Cy3–Pol δ

Pol δ was prepared in *S. cerevisiae* as previously described [4] and subsequently dialyzed into 250 mM NaCl, 5% (*v/v*) glycerol, 50 mM potassium glutamate, 25 mM HEPES pH 7.5, and 2 mM dithiothreitol. Following dialysis Pol δ was labelled with a 5-fold molar excess of Cy3–NHS (GE Healthcare) for 5 min at 4°C. Excess dye was removed by five buffer exchange steps through a centrifugal filter (50K MWCO; Millipore) following the manufacturer's instructions. Labelled Cy3–Pol δ was frozen in liquid N_2 and stored in aliquots at –80°C. The degree of labelling was measured to be 5 fluorophores per Pol δ holoenzyme by UV/vis spectrophotometry.

Preparation of AF647–Pol δ^{32-}

Alexa Fluor 647 (Invitrogen), was used to label Pol δ^{32-}. Labelling reactions were carried out using 3-fold molar excess of dye with 58.5 μM Pol δ^{32-} in 320 μL of 30 mM Tris-HCl pH 7.6, 2 mM dithiothreitol, 300 mM NaCl, 50 mM potassium glutamate, 10% (*v/v*) glycerol for 10 min at 4°C with gentle rotation. Immediately following the coupling, excess dye was removed from sequential elutions from two 0.5 mL Zeba spin desalting columns (7K MWCO; Thermofisher) following the manufacturer's instructions equilibrated in 30 mM Tris-HCl pH 7.6, 2 mM dithiothreitol, 300 mM NaCl, 50 mM potassium glutamate, 10% (*v/v*) glycerol. Labelled AF647–Pol δ^{32-} was frozen in liquid N_2 and stored in aliquots at –80°C.

The degree of labelling was measured to be 1 fluorophore per Pol δ^{32-} holoenzyme by UV/vis spectrophotometry.

Preparation of AF647–RPA

Alexa Fluor 647 (Invitrogen), was used to label RPA. Labelling reactions were carried out using 5-fold molar excess of dye with 45 μM RPA in 550 μL of 50 mM Tris-HCl pH 7.6, 3 mM dithiothreitol, 1mM EDTA, 200 mM NaCl, 10% (*v*/*v*) glycerol for 2 hours at 23°C with gentle rotation. Immediately following the coupling, excess dye was removed by gel filtration at 1 mL/min through a column (1.5 × 10 cm) of Sephadex G-25 (GE Healthcare), equilibrated in gel filtration buffer (50 mM Tris-HCl pH 7.6, 3 mM dithiothreitol, 1mM EDTA, 200 mM NaCl, 20% (*v*/*v*) glycerol). Labelled AF647–RPA was frozen in liquid N_2 and stored as single use aliquots at –80°C. The degree of labelling was measured to be 1 fluorophore per RPA trimer by UV/vis spectrophotometry.

Linear forked doubly-tethered DNA substrates

To make the linear fork DNA substrate, plasmid pSupercos1 DNA [37] was linearized overnight at 37°C with 100 U of *Bst*XI in 1 x Buffer 3.1 (New England Biolabs). The 18,284 bp fragment was purified with a Wizard SV gel and PCR clean up kit (Promega) and the concentration was measured. The fork junction was constructed by annealing 15.3 pmol of 160Ld, 91.8 pmol 99Lg, 1530 pmol of fork primer (Extended Data Table 1) by heating at 94°C for 5 min before slowly cooling. Similarly, the biotinylated blocking duplex was generated by annealing 5.3 pmol of blockingLd and blockingLg by heating at 94°C for 5 min before slowly cooling. 1.5 pmol of the 18,284 bp linear DNA template was ligated to the pre-annealed fork junction and biotinylated blocking duplex in 1 x T4 ligase buffer and 2000 U of T4 ligase (New England Biolabs) overnight at 16°C. Linear fork DNA substrates were purified from excess DNA oligonucleotides by adjusting NaCl to 300 mM and loaded by gravity onto a Sepharose 4B (Sigma; 1 × 25 cm) column, equilibrated in gel filtration buffer

(10 mM Tris-HCl pH 8.0, 1 mM EDTA, and 300 mM NaCl). Biotinylated linear DNA substrates eluted as a single peak in the column void volume, fractions under the peak were analysed by agarose gel electrophoresis. Fractions containing linear DNA substrates were pooled and dialysed overnight in 2 L of sterilised TE buffer, concentrated 2-fold in a vacuum concentrator and the concentration measured. Aliquots were stored at –80°C.

Single-molecule DNA replication assays

Flow cells were prepared as described previously [9,38]. Briefly, a polydimethylsiloxane (Sylgard®) lid was placed on top of a PEG-biotin-functionalised microscope slide (24 × 24 mm, Marienfeld) to create a 1-mm-wide and 100-µm-high flow channel. Polyethyleme tubes (PE-60: 0.76-mm inlet diameter and 1.22-mm outer diameter, Walker Scientific) were inserted to allow for a buffer flow. To help prevent nonspecific interactions of proteins and DNA with the surface, the chamber was blocked with blocking buffer (50 mM Tris-HCl pH 7.6, 50 mM KCl, 2% (*v/v*) Tween-20). The forked DNA substrates (20 pM) were flowed through the chamber for 20 min at 17 µL/min in the presence of 200 µM Chloroquine (Sigma) [39]. The DNA was visualised by flowing in replication buffer (25 mM Tris-HCl, pH 7.6, 10 mM magnesium acetate, 50 mM potassium glutamate, 40 µg/mL BSA, 0.1 mM EDTA, 5 mM dithiothreitol, and 0.0025% (*v/v*) Tween-20) with 150 nM S.O. (Invitrogen).

The replication reaction was performed in stages. First, 30 nM CMG was loaded at 10 µL/min in CMG loading buffer (25 mM Tris-HCl, pH 7.6, 10 mM magnesium acetate, 250 mM potassium glutamate, 40 µg/mL BSA, 0.1 mM EDTA, 5 mM dithiothreitol, and 0.0025% (vol/vol) Tween-20), with 60 nM Mcm10 and 400 µM ATP. Then, replication reactions were initiated by introducing 60 nM Mcm10, 20 nM Pol ε (unless specified otherwise), 20 nM Pol δ (unless specified otherwise), 20 nM Pol α (unless specified otherwise), 20 nM Ctf4, 20 nM PCNA, 20 nM or 2nM RFC, 200 nM RPA, and 30 nM MTC in replication buffer supplemented with 5 mM ATP, 60 µM dCTP, dGTP, dATP, and dTTP, and 250 µM dCTP,

GTP, ATP, and UTP, and 150 nM S.O. All single-molecule assays were carried out on an inverted microscope (Nikon Eclipse Ti-E) fitted with a CFI Apo TIRF 100× oil-immersion objective (NA 1.49, Nikon). The tempature was manintained at 30°C by an electrically heated chamber (Okolab).

dsDNA was visualised every 10 s for 30 min by exciting the S.O. with a 568-nm laser (Coherent, Sapphire 568–200 CW) at 80 mW/cm^2. The red fluorescently labelled proteins were excited at 80 mW/cm^2 (800 W/cm^2 during a FRAP pulse) with a 647-nm laser (Coherent, Obis 647–100 CW). The AF488–Pol ε was visualised with a 488-nm laser at 140 mW/cm^2. The signals were spectrally separated using appropriate filter sets (Chroma) and fluorescence signals collected on an Evolve 512 Delta EMCCD (Photometics). Typically, nine fields of view (five for the FRAP experiments) were selected for imaging. Single-molecule experimental results were derived from three or four technical replicates for each experimental condition.

Determination of RPA binding footprint

Flow cells were prepared as described above. Oligos 57-mer or 99Lg (Extended Data Table 1) were incubated with AF647–RPA in replication buffer for 10 min at 25°C. DNA–RPA complexes were introduced on the surface of the flowcell and washed with 100 μL of replication buffer. The AF647–RPA were excited at 80 mW/cm^2 with a 647-nm laser (Coherent, Obis 647–100 CW). Imaging was carried out as described in 'Single-molecule DNA replication assays'.

Measurement of the stoichiometry of fluorescently labelled proteins at the replisome

The average intensity of a single labelled proteins (Pol ε, Pol δ, or RPA) were calculated by immobilisation on the surface of a cleaned microscope coverslip in replication buffer at 6 pM. The imaging was under the same conditions as used during the single-molecule

replication experiments. We calculated the integrated intensity for every fluorescent protein in a field of view after applying a local background subtraction [22]. The histograms obtained were fit with a Gaussian distribution function using MATLAB 2016b, to give a mean intensity. We calculated the total number of Pol ε, Pol δ, or RPA at every time point during DNA replication by dividing their intensities by the intensity of a single Pol ε, Pol δ, or RPA molecule. Subsequent histograms were fit to Gaussian distribution using MATLAB 2016b.

Analysis of single-molecule replication kinetics and protein dynamics

All analysis was done with ImageJ/Fiji (1.51w) and Matlab 2016b, using in-house built plugins. The rate of replication of a single molecule was obtained by first tracking the position of the leading-strand spot using the Linear-motion LAP tracker in TrackMate v3.6.0 [16]. Individual rate segments were identified using kinetic change-point analysis [22,33,40,41]. The rates obtained from this algorithm were weighted by the DNA segment length, to reflect the number of nucleotides that were synthesised at this rate. This places more significance on the longer rate segments, as they have a higher signal-to-noise ratio compared with shorter segments [22].

To measure the intensity of the leading-strand spot at the replication fork, we tracked the position of the leading-strand spot and integrated the intensity for all colours simultaneously over time. To obtain the characteristic exchange time τ from the FRAP experiments, the data were fit with a FRAP recovery function correcting for photobleaching [9,10,24] (Formula 1, where a is the amplitude of photobleaching, t_b is the photobleaching time (measured in Extended Data Fig. 7), and I_0 is the number of polymerases at the fork at steady state).

$$I = ae^{-\frac{1}{\tau_b}t} + \mathrm{I}_0(1 - \mathrm{e}^{-\frac{1}{\tau}t}) \qquad (1)$$

The maximum exchange rate was obtained by fitting the data with a hyperbolic equation (Formula 2, where R is the exchange rate, R_{max} is the maximum exchange rate, [Pol] is the polymerase concentration, and K_b is the characteristic binding constant).

$$R = \frac{R_{max} * [Pol]}{K_b + [Pol]} \quad (2)$$

All home-built ImageJ plugins used in this study are freely available on the Github repository for Single-molecule/Image analysis tools (https://github.com/SingleMolecule) or available upon request.

References

1 Bell, S. P. & Labib, K. Chromosome Duplication in *Saccharomyces cerevisiae*. *Genetics* **203**, 1027-1067, doi:10.1534/genetics.115.186452 (2016).

2 Langston, L. D. *et al.* CMG helicase and DNA polymerase ε form a functional 15-subunit holoenzyme for eukaryotic leading-strand DNA replication. *Proceedings of the National Academy of Sciences of the United States of America* **111**, 15390-15395, doi:10.1073/pnas.1418334111 (2014).

3 Sun, J. *et al.* The architecture of a eukaryotic replisome. *Nature structural & molecular biology* **22**, 976-982, doi:10.1038/nsmb.3113 (2015).

4 Georgescu, R. E. *et al.* Mechanism of asymmetric polymerase assembly at the eukaryotic replication fork. *Nature structural & molecular biology* **21**, 664-670, doi:10.1038/nsmb.2851 (2014).

5 Gambus, A. *et al.* A key role for Ctf4 in coupling the MCM2–7 helicase to DNA polymerase α within the eukaryotic replisome. *The EMBO journal* **28**, 2992-3004, doi:10.1038/emboj.2009.226 (2009).

6 Warren, E. M., Huang, H., Fanning, E., Chazin, W. J. & Eichman, B. F. Physical interactions between Mcm10, DNA, and DNA polymerase alpha. *The Journal of biological chemistry* **284**, 24662-24672, doi:10.1074/jbc.M109.020438 (2009).

7 Geertsema, H. J., Kulczyk, A. W., Richardson, C. C. & van Oijen, A. M. Single-molecule studies of polymerase dynamics and stoichiometry at the bacteriophage T7 replication machinery. *Proceedings of the National Academy of Sciences of the United States of America* **111**, 4073-4078, doi:10.1073/pnas.1402010111 (2014).

8 Loparo, J. J., Kulczyk, A. W., Richardson, C. C. & van Oijen, A. M. Simultaneous single-molecule measurements of phage T7 replisome composition and function reveal the mechanism of polymerase exchange. *Proceedings of the National Academy of Sciences of the United States of America* **108**, 3584-3589, doi:10.1073/pnas.1018824108 (2011).

9 Lewis, J. S. *et al.* Single-molecule visualization of fast polymerase turnover in the bacterial replisome. *eLife* **6**, doi:10.7554/eLife.23932 (2017).

10 Beattie, T. R. *et al.* Frequent exchange of the DNA polymerase during bacterial chromosome replication. *eLife* **6**, doi:10.7554/eLife.21763 (2017).

11 Liao, Y., Li, Y., Schroeder, J. W., Simmons, L. A. & Biteen, J. S. Single-molecule DNA polymerase dynamics at a bacterial replisome in live cells. *Biophysical journal* **111**, 2562-2569, doi:10.1016/j.bpj.2016.11.006 (2016).
12 Huang, M. E., Le Douarin, B., Henry, C. & Galibert, F. The *Saccharomyces cerevisiae* protein YJR043C (Pol32) interacts with the catalytic subunit of DNA polymerase alpha and is required for cell cycle progression in G2/M. *Molecular & general genetics : MGG* **260**, 541-550 (1999).
13 Johansson, E., Garg, P. & Burgers, P. M. The Pol32 subunit of DNA polymerase δ contains separable domains for processive replication and proliferating cell nuclear antigen (PCNA) binding. *The Journal of biological chemistry* **279**, 1907-1915, doi:10.1074/jbc.M310362200 (2004).
14 Georgescu, R. E. *et al.* Reconstitution of a eukaryotic replisome reveals suppression mechanisms that define leading/lagging strand operation. *eLife* **4**, e04988, doi:10.7554/eLife.04988 (2015).
15 Ganji, M. *et al.* Real-time imaging of DNA loop extrusion by condensin. *Science (New York, N.Y.)* **360**, 102-105, doi:10.1126/science.aar7831 (2018).
16 Tinevez, J. Y. *et al.* TrackMate: An open and extensible platform for single-particle tracking. *Methods (San Diego, Calif.)* **115**, 80-90, doi:10.1016/j.ymeth.2016.09.016 (2017).
17 Tourriere, H., Versini, G., Cordon-Preciado, V., Alabert, C. & Pasero, P. Mrc1 and Tof1 promote replication fork progression and recovery independently of Rad53. *Molecular cell* **19**, 699-706, doi:10.1016/j.molcel.2005.07.028 (2005).
18 Szyjka, S. J., Viggiani, C. J. & Aparicio, O. M. Mrc1 is required for normal progression of replication forks throughout chromatin in *S. cerevisiae*. *Molecular cell* **19**, 691-697, doi:10.1016/j.molcel.2005.06.037 (2005).
19 Hodgson, B., Calzada, A. & Labib, K. Mrc1 and Tof1 regulate DNA replication forks in different ways during normal S phase. *Molecular biology of the cell* **18**, 3894-3902, doi:10.1091/mbc.e07-05-0500 (2007).
20 Aria, V. & Yeeles, J. T. P. Mechanism of bidirectional leading-strand synthesis establishment at eukaryotic DNA replication origins. *Molecular cell*, doi:10.1016/j.molcel.2018.10.019 (2018).
21 Sekedat, M. D. *et al.* GINS motion reveals replication fork progression is remarkably uniform throughout the yeast genome. *Molecular systems biology* **6**, 353, doi:10.1038/msb.2010.8 (2010).
22 Lewis, J. S. *et al.* Single-molecule visualization of *Saccharomyces cerevisiae* leading-strand synthesis reveals dynamic interaction between MTC and the replisome. *Proceedings of the National Academy of Sciences of the United States of America* **114**, 10630-10635, doi:10.1073/pnas.1711291114 (2017).
23 Yeeles, J. T. P., Janska, A., Early, A. & Diffley, J. F. X. How the eukaryotic replisome achieves rapid and efficient DNA replication. *Molecular cell* **65**, 105-116, doi:10.1016/j.molcel.2016.11.017 (2017).
24 Spenkelink, L. M. *et al.* Recycling of single-stranded DNA-binding protein by the bacterial replisome. *Nucleic acids research*, doi:10.1093/nar/gkz090 (2019).
25 Schauer, G. D. & O'Donnell, M. E. Quality control mechanisms exclude incorrect polymerases from the eukaryotic replication fork. *Proceedings of the National Academy of Sciences of the United States of America* **114**, 675-680, doi:10.1073/pnas.1619748114 (2017).
26 Simon, A. C. *et al.* A Ctf4 trimer couples the CMG helicase to DNA polymerase α in the eukaryotic replisome. *Nature* **510**, 293-297, doi:10.1038/nature13234 (2014).

27 Kurat, C. F., Yeeles, J. T. P., Patel, H., Early, A. & Diffley, J. F. X. Chromatin controls DNA replication origin selection, lagging-strand synthesis, and replication fork rates. *Molecular cell* **65**, 117-130, doi:10.1016/j.molcel.2016.11.016 (2017).
28 Conti, C. *et al.* Replication fork velocities at adjacent replication origins are coordinately modified during DNA replication in human cells. *Molecular biology of the cell* **18**, 3059-3067, doi:10.1091/mbc.e06-08-0689 (2007).
29 Park, K., Debyser, Z., Tabor, S., Richardson, C. C. & Griffith, J. D. Formation of a DNA loop at the replication fork generated by bacteriophage T7 replication proteins. *The Journal of biological chemistry* **273**, 5260-5270 (1998).
30 Chastain, P. D., 2nd, Makhov, A. M., Nossal, N. G. & Griffith, J. Architecture of the replication complex and DNA loops at the fork generated by the bacteriophage T4 proteins. *The Journal of biological chemistry* **278**, 21276-21285, doi:10.1074/jbc.M301573200 (2003).
31 Hamdan, S. M., Loparo, J. J., Takahashi, M., Richardson, C. C. & van Oijen, A. M. Dynamics of DNA replication loops reveal temporal control of lagging-strand synthesis. *Nature* **457**, 336-339, doi:10.1038/nature07512 (2009).
32 Bermek, O., Willcox, S. & Griffith, J. D. DNA replication catalyzed by herpes simplex virus type 1 proteins reveals trombone loops at the fork. *The Journal of biological chemistry* **290**, 2539-2545, doi:10.1074/jbc.M114.623009 (2015).
33 Duderstadt, K. E. *et al.* Simultaneous real-time imaging of leading and lagging strand synthesis reveals the coordination dynamics of single replisomes. *Molecular cell* **64**, 1035-1047, doi:10.1016/j.molcel.2016.10.028 (2016).
34 Langston, L. D. *et al.* Mcm10 promotes rapid isomerization of CMG–DNA for replisome bypass of lagging strand DNA blocks. *eLife* **6**, doi:10.7554/eLife.29118 (2017).
35 Yin, J., Lin, A. J., Golan, D. E. & Walsh, C. T. Site-specific protein labeling by Sfp phosphopantetheinyl transferase. *Nature protocols* **1**, 280-285, doi:10.1038/nprot.2006.43 (2006).
36 Zhou, Z. *et al.* Genetically encoded short peptide tags for orthogonal protein labeling by Sfp and AcpS phosphopantetheinyl transferases. *ACS chemical biology* **2**, 337-346, doi:10.1021/cb700054k (2007).
37 van Loenhout, M. T., de Grunt, M. V. & Dekker, C. Dynamics of DNA supercoils. *Science (New York, N.Y.)* **338**, 94-97, doi:10.1126/science.1225810 (2012).
38 Geertsema, H. J., Duderstadt, K. E. & van Oijen, A. M. Single-molecule observation of prokaryotic DNA replication. *Methods in molecular biology (Clifton, N.J.)* **1300**, 219-238, doi:10.1007/978-1-4939-2596-4_14 (2015).
39 Yardimci, H., Loveland, A. B., Habuchi, S., van Oijen, A. M. & Walter, J. C. Uncoupling of sister replisomes during eukaryotic DNA replication. *Molecular cell* **40**, 834-840, doi:10.1016/j.molcel.2010.11.027 (2010).
40 Watkins, L. P. & Yang, H. Detection of intensity change points in time-resolved single-molecule measurements. *The journal of physical chemistry. B* **109**, 617-628, doi:10.1021/jp0467548 (2005).
41 Hill, F. R., van Oijen, A. M. & Duderstadt, K. E. Detection of kinetic change points in piece-wise linear single molecule motion. *The Journal of chemical physics* **148**, 123317, doi:10.1063/1.5009387 (2018).

Acknowledgements

This work was supported by Australian Research Council Grant DP180100858, Australian Laureate Fellowship FL140100027 (to A.M.v.O.), NIH Grant GM-115809 (to M.E.O.), and Howard Hughes Medical Institute (M.E.O.). We thank Dr. Dan Zhang of the O'Donnell lab for purification of CMG, Cees Dekker for pSuperCos1, and Daniel Zalami for his help in setting up Trackmate.

Author Contributions

J.S.L and L.M.S equally contributed to this work and are listed in random order. J.S.L and L.M.S designed, carried out, and analysed single-molecule replication assays; G.D.S and O.Y. isolated, purified, and fluorescently labelled proteins; V.N., C.M., and C.K. carried out single-molecule replication assays. G.K. fluorescently labelled RPA. J.S.L, L.M.S, A.M.v.O., G.D.S, and M.E.O designed the research and wrote the article. All authors discussed the results and commented on the manuscript.

Author Information

Reprints and permissions information is available at www.nature.com/reprints. The authors declare no competing financial interests. Correspondence and requests for materials should be addressed to A.M.v.O (vanoijen@uow.edu.au) or M.E.O. (odonnel@rockefeller.edu).

ORCIDs

J.S.L.: 0000-0002-9945-6133; L.M.S.: 0000-0002-5511-8757; G.K: 0000-0003-4466-2279; C.M.: 0000-0002-3300-7829; C.K.: 0000-0002-0985-6206; M.E.O.: 0000-0001-9002-4214; A.M.v.O.: 0000-0002-1794-5161

Figure legends

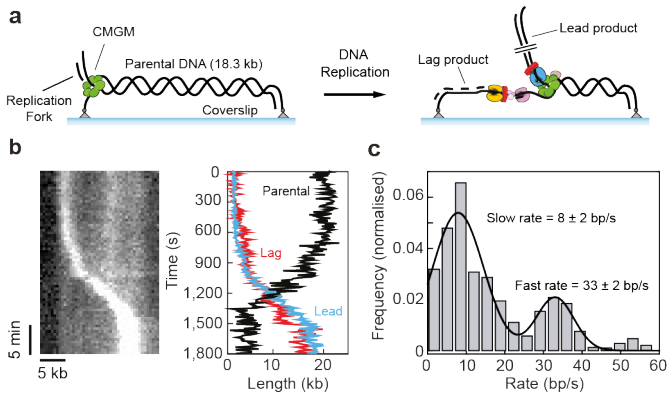

Fig. 1: Single-molecule visualisation of DNA synthesis. a, Schematic representation of DNA replication assay (see methods for details). **b,** (left) Kymograph showing DNA replication on a single DNA substrate. The leading-strand tail appears as a bright spot that moves in a unidirectional manner, while simultaneously increasing in intensity. (right) Length of the lagging strand ('Lag'), leading strand ('Lead') and parental DNA ('Parental') as a function of time, measured by the integrated intensity of the dsDNA. **c,** Single-molecule rate distribution. The bimodal distribution was fit with the sum of two Gaussians (black line) with rates of 8 ± 2 bp/s and 33 ± 2 bp/s (n = 96 molecules). Errors represent S.E.M.

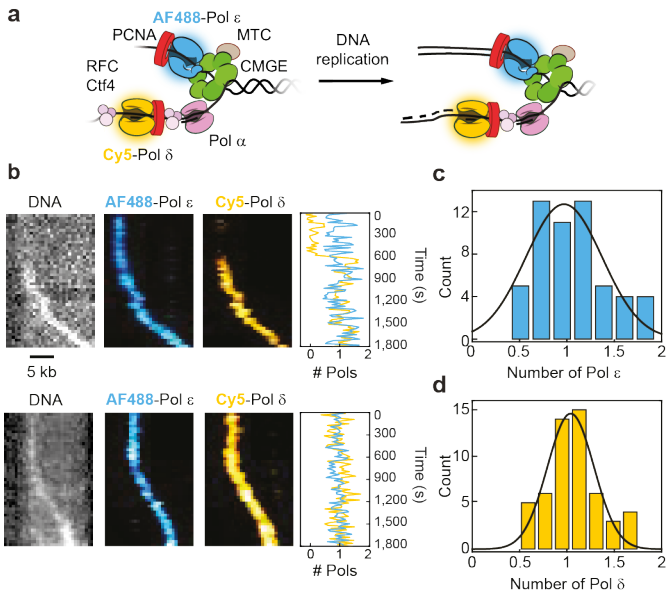

Fig. 2: Visualisation of Pol ε and Pol δ. a, Schematic representation of the replisome with labelled polymerases. **b,** Example kymographs showing the DNA, AF488–Pol ε, Cy5–Pol δ, and the polymerase intensities as a function of time. Both polymerases co-localise with the leading-strand spot. **c,** Distribution of the number of Pol ε at the fork (n = 55). A Gaussian fit (black line) gives 1.0 ± 0.2 (mean ± S.E.M.) Pol ε per replisome. **d,** Distribution of the number of Pol δ at the fork (n = 55). A Gaussian fit (black line) gives 1.0 ± 0.1 (mean ± S.E.M.) Pol δ per replisome.

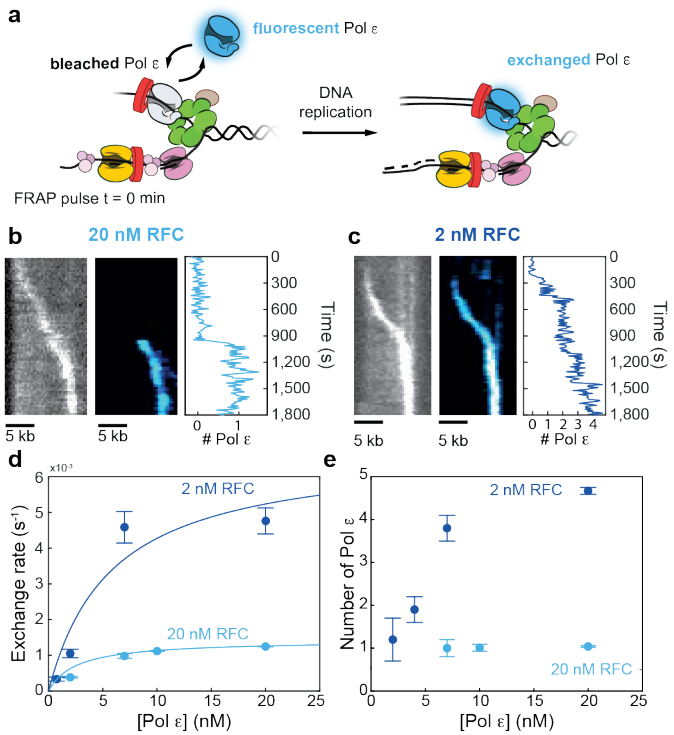

Fig. 3: Pol ε dynamics. a, Schematic representation of the FRAP assay. **b,** Example kymograph showing the DNA (left), LD650–Pol ε (middle), and the LD650–Pol ε intensity at the fork (right). **c**, Example kymograph using a ten-fold lower [RFC]. The Pol ε exchange is much faster than in panel **b**, and multiple polymerases are present at the fork. **d,** Exchange rate as a function of Pol ε concentration. The lines represent hyperbolic fits, giving a maximum exchange rate of $(1.4 \pm 0.5)\times10^{-3}$ s^{-1} (mean ± error of the fit) at 20 nM RFC (light blue) and $(7 \pm 5)\times10^{-3}$ s^{-1} (mean ± error of the fit) at 2 nM RFC (dark blue). **e,** Number of

Pol ε at the fork as a function of Pol ε concentration, at 20 nM RFC (light blue) and 2 nM RFC (dark blue). Error bars represent S.E.M.

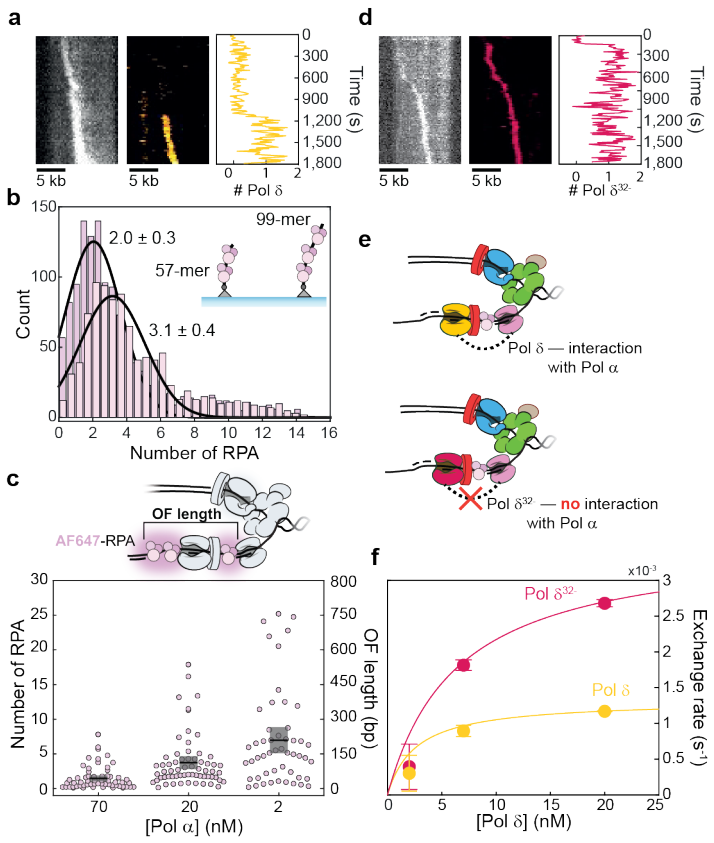

Fig. 4: Pol δ dynamics. a, Example kymograph showing the DNA and Cy5–Pol δ, and corresponding Cy5–Pol δ intensity at the fork. **b,** Histograms of the number of RPA molecules binding to either a 57-mer (purple, n = 1299) and 99-mer oligo (pink, n = 939). From this we find an average ssDNA–RPA footprint of 30 ± 2 nt. Errors represents S.E.M. **c,** (top) Schematic representation showing the relationship between the number of RPA molecules and Okazaki-fragment length. (bottom) scatter plots of the number of RPA for 70 nM (1.5 ± 0.3; n = 60), 20 nM (3.7 ± 0.5; n = 64), and 2 nM (7.0 ± 0.9; n = 51) Pol α. The black line and grey box represent the mean and S.E.M. **d,** Example kymograph showing the DNA and AF647–Pol δ^{32-}, and corresponding AF647–Pol δ^{32-} intensity at the fork. **e,** Schematic representation of interactions of Pol δ with the replisome. **f,** Exchange rate as a function of polymerase concentration with Pol δ (yellow) and Pol δ^{32-} (magenta). The lines

represent hyperbolic fits, giving a maximum exchange rate of $(1 \pm 3)\times10^{-3}$ (mean ± error of the fit) for Pol δ (yellow) and $(4 \pm 8)\times10^{-3}$ (mean ± error of the fit) Pol δ^{32-} (magenta).

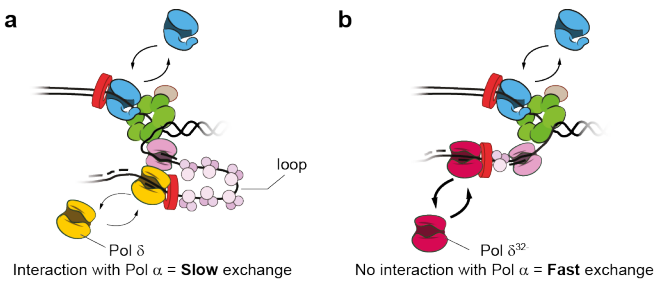

Fig. 5: Compositional plasticity at the eukaryotic replication fork. Pol ε and Pol δ exchange in a concentration-dependent manner. **a,** Pol δ is linked to CMG through interaction with Pol α through its Pol 32 subunit, and possibly additional unidentified interactions, resulting in slow exchange. **b,** Pol δ^{32-} does not interact with Pol α and exchanges 2.5-fold faster.

Extended Data

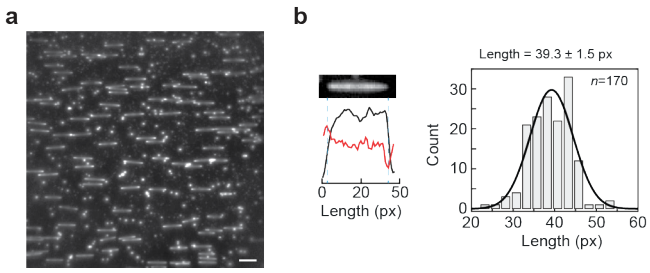

Extended Data Fig 1: Linear dsDNA substrates. a, Representative field of view showing doubly tethered DNA substrates in the absence of any buffer flow. Scale bar = 20 kb. **b**, Calibration of the length of the DNA substrates under our experimental conditions. Error represents S.E.M. *n* = number of molecules.

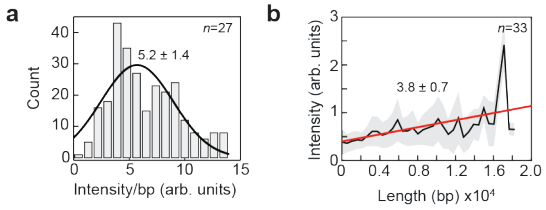

Extended Data Fig 2: DNA Intensity quantification. a, Fluorescence intensity per base pair in the leading-strand spot. **b,** Fluorescence intensity per base pair from the 18.3 kb substrate. Error represents S.E.M. *n* = number of molecules.

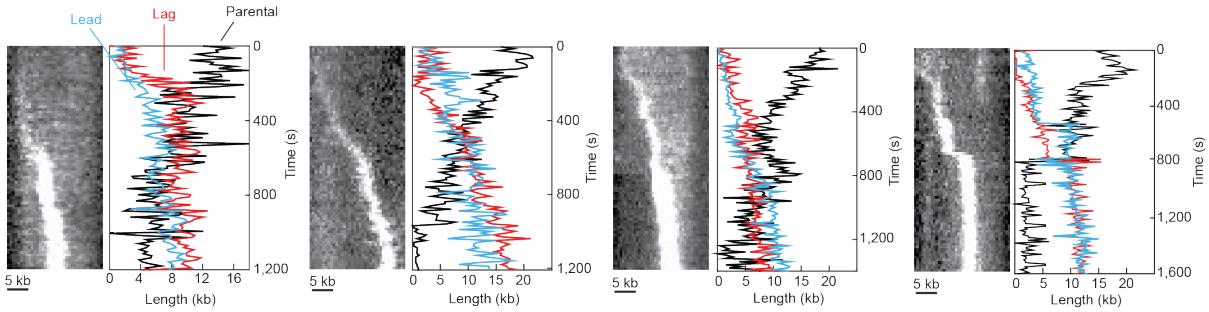

Extended data Fig. 3: Simultaneous leading- lagging-strand synthesis. Representative kymographs and corresponding graphs showing length of the lagging-strand ('Lag'), leading-

strand (‘Lead’) and parental DNA (‘Parental’) as a function of time, measured by the integrated intensity of the dsDNA.

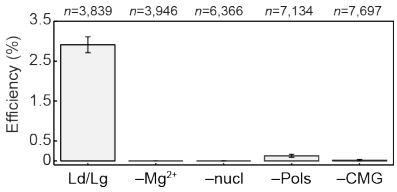

Extended data Fig. 4: Negative controls. The replication efficiency was defined as the number of templates that showed replication, divided by the total number of observed DNA substrates. Error bars represent S.E.M. *n* = number of DNA substrates.

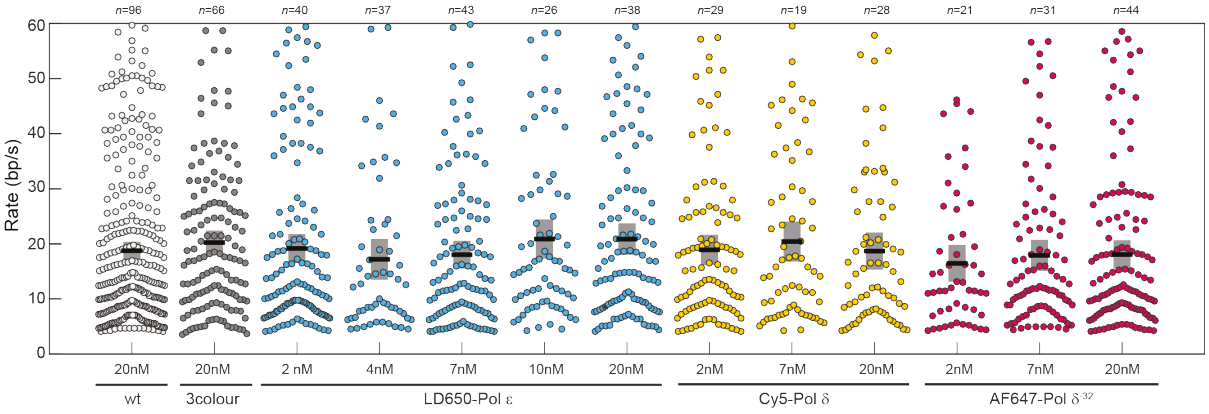

Extended data Fig. 5: Comparison of replication rates at different concentrations of polymerases. Scatter plots of the single-molecule rate segments from wild-type polymerases (white), 20 nM AF488–Pol ε and Cy5–Pol δ (grey), increasing concentrations of LD650–Pol ε (blue), increasing concentrations of Cy5–Pol δ (yellow), and increasing concentrations of AF647–Pol δ^{32-} (red). The black line and grey box represent the mean and S.E.M. *n* = the number of molecules.

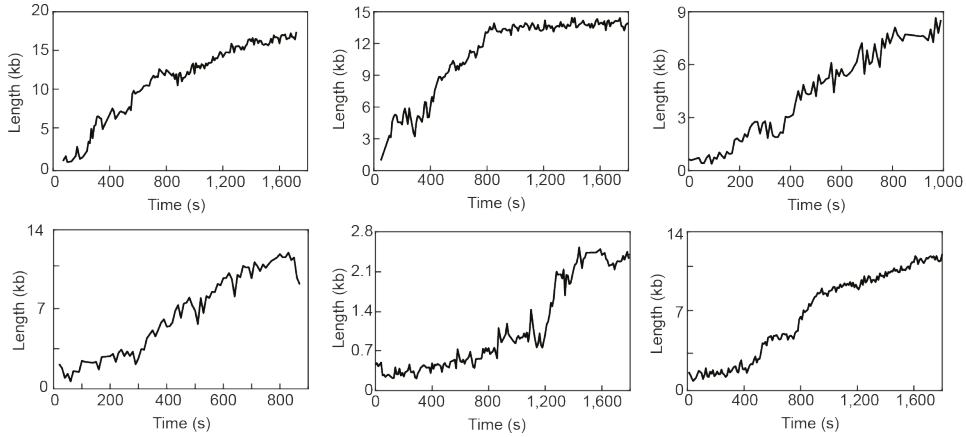

Extended data Fig. 6: Example trajectories. Distance travelled as a function of time for six representative single molecules.

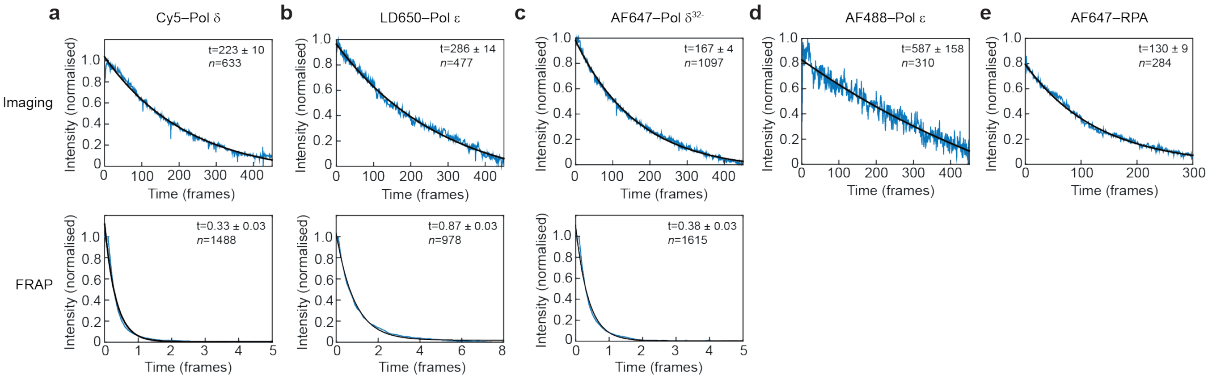

Extended Data Fig. 7: Quantification of photobleaching kinetics of fluorescently labelled polymerases. The normalised average intensity as a function of time (in frames) under imaging conditions (top) and FRAP photobleaching-pulse conditions (bottom) for **a,** Cy5–Pol δ **b,** LD650–Pol ε, **c,** AF647–Pol δ, **d,** AF488–Pol ε, and **e,** AF647–RPA. Errors represent error of the fit.

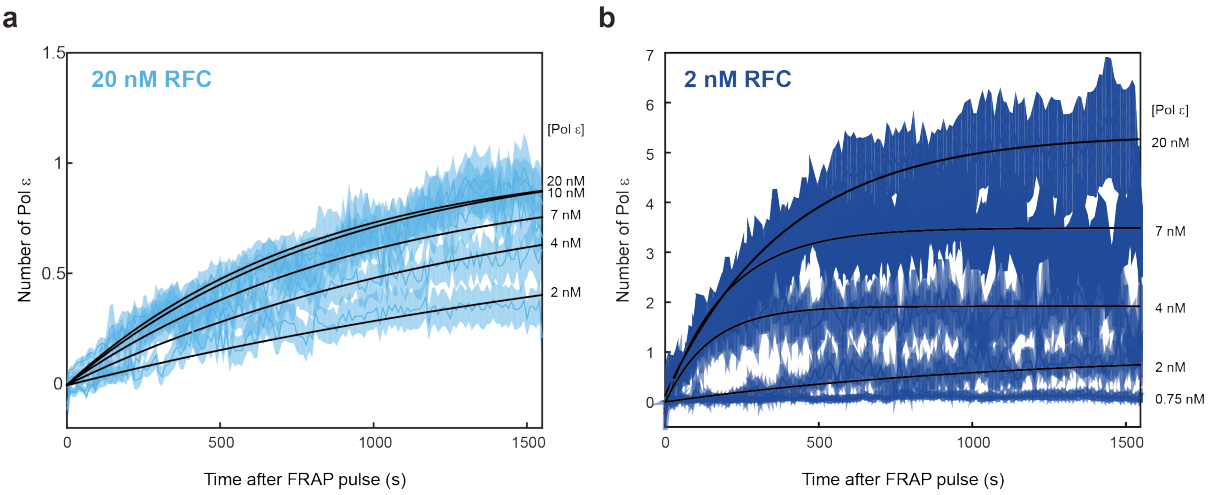

Extended Data Fig. 8: FRAP recovery curves for Pol ε. Average number of Pol ε at the replication fork over time after the FRAP pulse for different concentrations of Pol ε at **a,** 20 nM RFC and **b,** 2 nM RFC. Fit using formula 1 (See methods for detailed explainations).

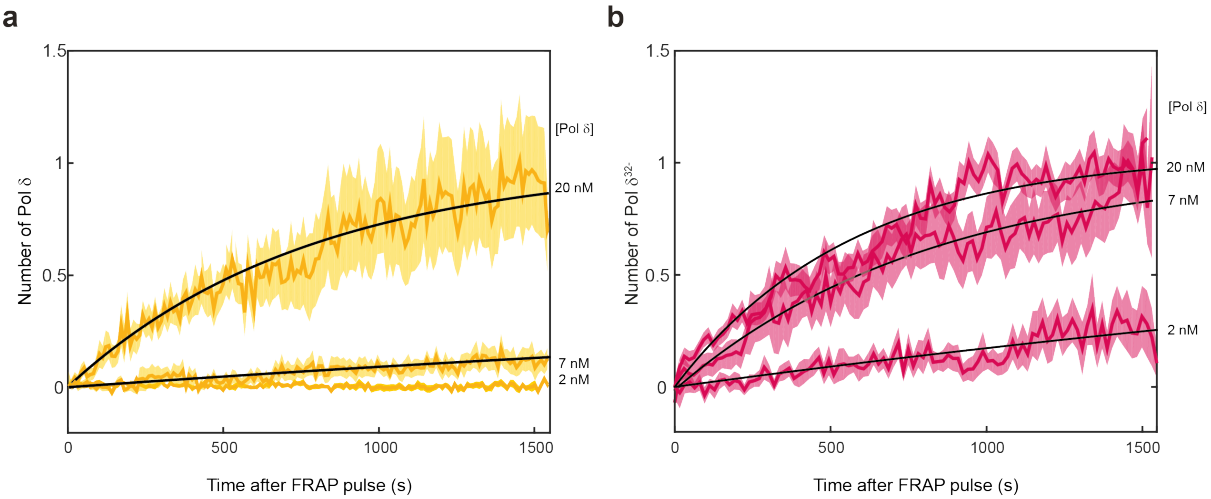

Extended Data Fig. 9: FRAP recovery curves for Pol δ. Average number of Pol δ at the replication fork over time after the FRAP pulse for **a,** different concentrations of Pol δ and **b,** different concentrations of Pol δ^{32-}. Fit using formula 1 (See methods for detailed explainations).

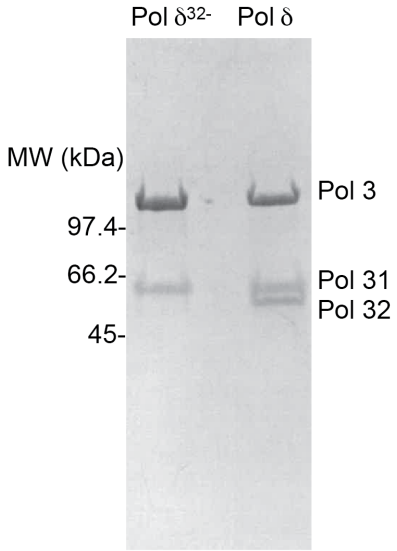

Extended data Fig 10: Coomassie blue stained SDS-PAGE gel of purified Pol δ and Pol δ^{32-}. (Lane 1) Pol δ holoenzyme lacking subunit 32 and (Lane 2) Pol δ holoenzyme.

Extended Data Table 1. Oligonucleotides used in this study.

Oligo name	Sequence (5′–3′)
BlockingLg	/phos/AGT CGC AGC TAT AGG TGG CAT TTC AG
Blocking Ld	/Bio/CTG AAA TGC CAC CTA TAG CTG CGA CTC ATG
160Ld	/Phos/ACC GAT GTG GTA GGA AGT GAG AAT TGG AGA GTG TGT TTT TTT TTT TTT TTT TTT TTT TTT TTT TTT TTT TTT TTT GAG GAA AGA ATG TTG GTG AGG GTT GGG AAG TGG AAG GAT GGG CTC GAG AGG TTT TTT TTT TTT TTT TTT TTT TTT TTT TTT T*T*T *T
Fork Primer	CCT CTC GAG CCC ATC CTT CCA CTT CCC AAC CCT CAC C
99Lg	/Bio/TTT TTT TTT TTT TTT TTT TTT TTT TTT TTT TTT TTT TTT TTT TTT TTT TTT TTT TTT CAC ACT CTC CAA TTC TCA CTT CCT ACC ACA TCG GTC GAT
57-mer	/Bio/TTT TTT TTT TTT TTT TTT TTC CTC TCG AGC CCA TCC TTC CAC TTC CCA ACC CTC ACC

*Represents phosphorothioate bond.

Supplementary Information

Supplementary Video 1. Single-molecule movie showing DNA replication on a single DNA substrate from example kymograph in Fig. 1b. Scale bar = 1 μm.